

Radiation-induced change of OH content in Yb-doped silica glass

Shuang Liu (刘双)^{1,2}, Shupeì Zheng (郑书培)^{1,2}, Ke Yang (杨科)^{1,2},
and Danping Chen (陈丹平)^{1,*}

¹Shanghai Institute of Optics and Fine Mechanics, Chinese Academy of Sciences, Shanghai 201800, China

²University of Chinese Academy of Sciences, Beijing 100049, China

*Corresponding author: dp-chen@siom.ac.cn

Received February 4, 2015; accepted April 8, 2015; posted online May 4, 2015

Yb-doped silica glasses containing low, medium, and high content of OH are prepared through nanoporous glass sintering technology. High-OH sample exhibits better X-ray irradiation resistivity than low- and medium-OH samples. After irradiation, OH content of low- and medium-OH samples increases 37.5% and 11%, respectively; in contrast, OH content of high-OH sample decreases dramatically. The different OH content changes among the samples are discussed regarding the proposed inter-conversion reactions involving Si-H and Si-OH during the irradiation.

OCIS codes: 060.2290, 160.2750, 160.5690, 350.5610.

doi: 10.3788/COL201513.060602.

Active silica fibers doped with rare-earth (RE) ions have been vastly developed recently^[1-5]. An important factor for this development comprises the superior properties of silica glass, namely, extremely low optical loss, and extraordinary chemical and mechanical strength^[6]. Although silica glass fibers are superior in many aspects, their radiation hardness still remains an important issue. Yb-doped silica fiber, which is nearly the most important fiber in the field of high-power fiber lasers, has shown photodarkening under near-IR pumping^[7-9]. Unfortunately, pump-induced photodarkening is difficult to study directly, because high-power and long-duration pumping is required to accumulate substantial pump-induced changes in the material. As an approximation, high-energy irradiation on bulk silica glass is adopted as an accelerated simulation of pumping irradiation on silica fibers^[8].

Numerous results concerning radiation darkening of silica glasses and fibers have been published. Additional absorbance induced by radiation is due to defect centers formed during exposure to irradiation^[8]. In addition, many methods have been proposed to address the radiation hardness of silica glasses and fibers. Generally, the methods can be grouped into two categories: (1) tailoring the material composition, such as codoping with fluorine, cerium, and phosphorous^[10,11]; (2) pre- or post-treatment techniques, such as pre-loading hydrogen, post-annealing, and photobleaching^[12-14]. Recently, Fu *et al.*^[15] demonstrated that passive (pure) silica glass with higher content of hydroxyl exhibits better radiation hardness under gamma-ray irradiation. Hydroxyl incorporation is simpler than pre- or post-treatment methods and exerts less effects on the material refractive index than codoping approaches. Active (RE-doped) silica glasses may also benefit from this hydroxyl incorporation approach, especially for active silica glass fibers that have harsh demand on the material refractive index^[16].

In the present work, X-ray irradiation responses of bulk Yb-doped silica glasses containing low-, medium-, and high-content OH are systematically investigated through optical absorption (OA) and radiation-induced absorbance (RIA). In particular, Fourier-transform IR (FTIR) spectroscopy is used to monitor hydroxyl contents in pristine and irradiated glasses. Based on the experimental results, reactions involving hydroxyl, hydride, and defect centers are discussed. It is demonstrated that Yb-doping exerts no significant effects on the role of OH groups of improving radiation hardness of silica glass.

Yb-doped silica glasses were prepared using the nanoporous glass sintering technique^[17,18]. The first step was leaching out the borate phase from phase-separated borosilicate glass. The obtained nanoporous silica glass powders were then impregnated in dopant solution with certain concentrations of ytterbium chloride and aluminum chloride. After drying and purifying, the doped powders were transferred into a vacuum furnace and were sintered at the temperature of 1750°C. The tailoring of hydroxyl content was realized through variations in the pre-treatment (drying temperature and duration) procedures of the solution-doped powders. The as-prepared transparent and dense silica glasses were sliced and polished for spectroscopy measurements. Thickness of the samples was 4.00 mm for OA measurements and 0.56 mm for FTIR measurements. Irradiated samples were obtained after irradiated the as-prepared samples with a Mo K α X-ray tube at 30 mA tube current and 40 kV tube voltage. The irradiation duration for each sample was set to 1 h.

Chemical compositions of Yb-doped silica glass samples were analyzed using inductively coupled plasma (ICP)-atomic emission spectroscopy (AES). Optical absorbance spectra within the range of 190–850 nm were obtained with a JASCO V-570 spectrometer. RIA spectra were

obtained by subtracting the OA spectra of pristine samples from that of the irradiated samples. FTIR spectra were recorded by using a Nicolet 6700 FT-IR spectrometer. All measurements were performed at room temperature.

Samples with low-, medium-, and high-OH are labeled as Samples A–C, respectively. Due to the large dimensions of the samples, the hydroxyl contents can be readily determined from the intensity of the hydroxyl IR band at 3673 cm^{-1} in the FTIR spectra^[19,20]. Three spectra were recorded for each sample for averaging. The accuracy of the calculation was estimated to be within 3 ppm^[21]. The calculated OH contents and the ICP–AES analysis results of the samples are summarized in Table 1. The difference in Yb concentrations of Samples A–C is due to different concentrations of the dopant solution used for solution impregnation procedure during the preparation processes.

All three samples were visually darkened after X-ray irradiation. Responses to X-ray irradiations (OA spectra and RIAs) of all three samples are illustrated in Fig. 1. Figure 1, inset, clearly shows that RIA decreases from Samples A–C as the initial OH content increases. This suggests that Yb-doped silica glass containing higher content OH exhibits better resistivity to X-ray irradiation.

Table 1. Chemical Compositions and Hydroxyl Contents^a

Sample	A	B	C
Yb content	2100	1000	1000
Al content	2100	2200	2200
Initial OH content	16	110	273

^aConcentrations in parts per million by weight.

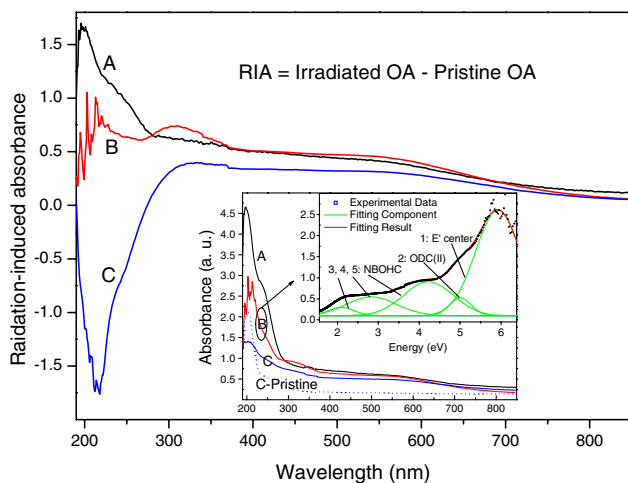


Fig. 1. RIA spectra. Inset, absorbance spectra of irradiated samples (solid lines) and pristine Sample C (dotted line). Gaussian decomposition of absorbance spectrum of irradiated Sample B is also given.

One forthright explanation for the enhanced resistivity is that hydroxyl in the glass suppresses or annihilates part of the radiation-induced defects. This assumption leads us to monitor the hydroxyl contents of the samples before and after irradiation.

The FTIR spectra and calculated OH contents of all the samples before and after irradiation are shown in Fig. 2. The overall range baseline shift may be due to measurement inaccuracy arising from the variations of the surface quality of the samples (inhomogeneity). In the inset, the IR bands of $\equiv\text{Si-OH}$ stretching mode are highlighted, with the baselines of the irradiated FTIR spectra shifted to their initial levels for comparison purpose. The calculated hydroxyl contents are also listed in Fig. 2, inset.

For Sample A, the hydroxyl content after irradiation increases from 16 ppm initially to 22 ppm, corresponding to the increase ratio of 37.5%. The increase ratio in Sample B drops to 11% as the initial OH content increases to 110 ppm. These increases of the hydroxyl groups are unusual since hydrogen molecules and atomic hydrogen are well-known for being able to annihilate defect centers in silica glass^[22–24]. Moreover, the hydroxyl content in high-OH Sample C decreases dramatically to 117 ppm from the initial value of 273 ppm.

The evolution of OH content change from Samples A–C is coincident with that of the 200–215 nm RIA peak as illustrated in Fig. 1. The 200–215 nm peaks should be associated with E' defect centers, which is characterized as an electron trapped on a silicon atom coordinated with three oxygen atoms (denoted as $\equiv\text{Si}\cdot$)^[14,25,26]. This attribution is supported by the Gaussian decomposition result shown in Fig. 1 in which a prominent Gaussian peak centered at 5.9 eV is demonstrated. Note that E' centers exist in our as-prepared samples prior to irradiation (Curve “C-Pristine” in Fig. 1, inset). This should be ascribed to the reducing sintering atmosphere and rapid-cooling fabrication process which led to imperfectly arranged atoms in silica glass network. Figure 1 indicates that the E'

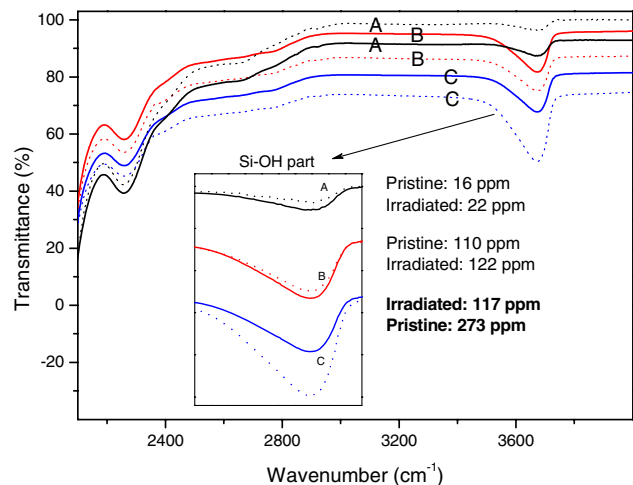
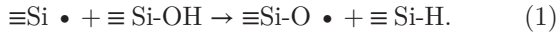


Fig. 2. FTIR spectra of pristine (dotted lines) and irradiated (solid lines) samples.

center concentration increases in Sample A, increases moderately in Sample B, and decreases dramatically in Sample C. Considering this coincidence in the evolution of OH content change and E' center absorbance, the following reaction may be valid during the irradiation



Equation (1) leads to formation of nonbridging oxygen hole centers (NBOHCs) and silicon hydride. NBOHC contains an oxygen dangling bond and is known for its OA bands in the visible range (400–700 nm) as shown in Fig. 1, inset. To be specific, three bands centering at 4.23, 2.83, and 2.09 eV are demonstrated by the Gaussian decomposition result; these three peaks are in agreement with those usually reported for the NBOHC, HC1, and HC2, respectively^[14,25–27]. HC1 comprises a hole trapped in a single $2p \pi$ orbital of a single nonbridging oxygen atom, whereas HC2 is a hole trapped on two nonbridging oxygen atoms bonded to the same silicon atom in glass network^[27]. Si-H groups can be evidenced by the IR band around 2250–2260 cm^{-1} in Fig. 2^[28].

Similar OH generation has been reported in Ref. [29]. They observed the generation of OH groups in dry silica glass after thermal treatment with 390°C for about 160 h in inert (helium) atmosphere. They interpreted the generation as a result of reaction between inherent (dissolved) hydrogen and preexisting peroxy linkage defects or regular Si-O-Si sites. However, in this work, the temperatures of the samples during irradiation never exceed 100°C and the irradiation duration is only 1 h. Besides, peroxy linkage defects are unlikely to exist given the oxygen-deficient sintering atmosphere during sample preparation. Thus, such intrinsic generation process is ruled out.

To explain the unusual increase of OH content in Samples A and B, conversion processes which can lead to $\equiv\text{Si-OH}$ production from some hydrogen-containing sources other than dissolved H_2 gas must be introduced. The most possible hydrogen-containing source should be $\equiv\text{Si-H}$, if no external hydrogen sources are considered. Therefore, the reverse reaction of Eq. (1) is also proposed



Actually, the assumption of this reverse process can be supported from the comparison of RIA spectra of Samples A and B. In Sample A, the E' center RIA peak is more intense than that of Sample B. However, the visible NBOHC RIA band of Sample A is weaker than that of Sample B (Fig. 1). Thus, we can deduce that more NBOHC in Sample A is consumed for producing E' center and $\equiv\text{Si-OH}$ following Eq. (2), resulting in a higher OH content increase ratio than Sample B.

Further evidence is provided by the difference FTIR results. As illustrated in Curve A of Fig. 3, the transmittance in $\equiv\text{Si-H}$ IR band increases after X-ray irradiation whereas the transmittance in $\equiv\text{Si-OH}$ IR band decreases. These contrary changes can be reasonably

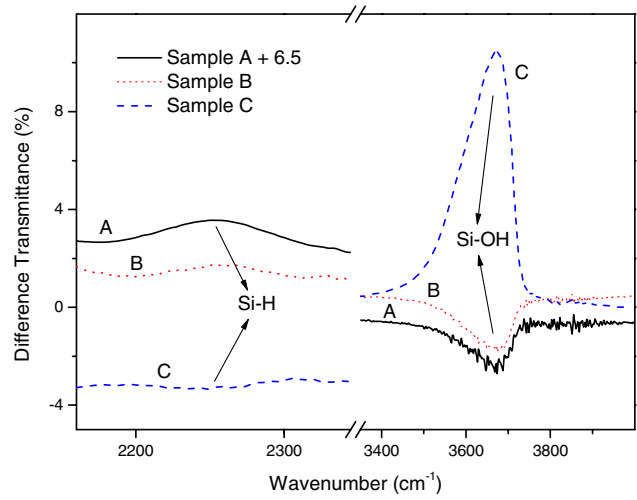


Fig. 3. Difference FTIR spectra; subtraction FTIR spectra of pristine samples from FTIR spectra of irradiated samples (difference-FTIR spectrum of Sample A is shifted 6.5 vertically for clarity).

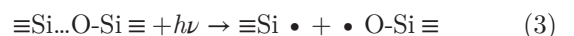
explained by Eq. (2). In Curve B of Fig. 3, the transmittance in the $\equiv\text{Si-H}$ IR band increase is not as prominent as in the case of Sample A, which is in line with a lower OH increase ratio in Sample B.

For Sample C, the transmittance in the $\equiv\text{Si-H}$ IR band decreases, suggesting that $\equiv\text{Si-H}$ group in Sample C increases after X-ray irradiation. This agrees with the proposed reaction [Eq. (1)], through which $\equiv\text{Si-H}$ is produced at the cost of the consumption of $\equiv\text{Si-OH}$.

Taking both the evolutions of OH content changes and RIA spectra into consideration, we conclude the enhancement of X-ray irradiation resistivity resulting from proper higher initial OH content of the Yb-doped silica glass.

The dominant reaction in Samples A and B is the reverse reaction [Eq. (2)], which leads to the increases of OH after irradiation. In Sample C, the dominant process turns to the forward reaction [Eq. (1)], resulting in the decrease of OH. The main reason leading to the change-over of the dominant reaction from Samples A/B to C may be explained according to the chemical equilibrium theory: higher (initial) content of OH, which is the reactant of the forward reaction [Eq. (1)] promotes the chemical equilibrium toward the right side; to the contrary, lesser initial OH favors the reverse reaction [Eq. (2)].

In addition, lower content initial OH in silica glass generally leads to more strained $\equiv\text{Si-O-Si} \equiv$ bonds in the silica glass network^[30]. This subsequently results in more defect centers, $\equiv\text{Si-O} \cdot$ and $\equiv\text{Si} \cdot$



This process may also exert a minor effect on the chemical equilibrium due to the differences in the stability of $\equiv\text{Si} \cdot$ and $\cdot \text{O-Si} \equiv$ defect centers.

In conclusion, low-, medium-, and high-OH Yb-doped silica glass samples are prepared by nanoporous glass

sintering technique. Their responses to X-ray irradiations are investigated using OA, RIA, and FTIR. A glass containing higher content of the initial OH exhibits better radiation resistivity. Moreover, the OH contents of low- and medium-OH samples increase, whereas the OH content of high-OH sample decreases dramatically. Considering the coincident evolutions of OH content changes and the RIA spectra, a conversion reaction involving Si-OH and Si-H and its reverse reaction are proposed: $\equiv\text{Si} \cdot + \equiv\text{Si-OH} \leftrightarrow \equiv\text{Si-O} \cdot + \equiv\text{Si-H}$. The dominant processes in Samples A/B and C are the reverse and the forward reaction, respectively. For practical applications, hydroxyl is well-known of being unfavorable for improving luminescence lifetime and intensity of active silica glass; however, proper hydroxyl incorporation may still be an acceptable compromise for better radiation hardness of silica glass and fiber especially when they are used in high-power laser engineering.

This work was supported by the National Natural Science Foundation of China under Grant Nos. 51272262 and 61405215.

References

1. C. Jauregui, J. Limpert, and A. Tünnermann, *Nat. Photonics* **7**, 861 (2013).
2. D. J. Richardson, J. Nilsson, and W. A. Clarkson, *J. Opt. Soc. Am. B* **27**, B63 (2010).
3. Y. Miao, H. Zhang, H. Xiao, and P. Zhou, *Chin. Opt. Lett.* **12**, 091403 (2014).
4. R. Su, P. Zhou, X. Wang, R. Tao, and X. Xu, *High Power Laser Sci. Eng.* **2**, e3 (2014).
5. W. Li, Q. Zhou, L. Zhang, S. Wang, M. Wang, C. Yu, S. Feng, D. Chen, and L. Hu, *Chin. Opt. Lett.* **11**, 091601 (2013).
6. J. Kirchhof, S. Unger, and A. Schwuchow, *Proc. SPIE* **4957**, 1 (2003).
7. J. J. Koponen, M. J. Söderlund, H. J. Hoffman, and S. K. T. Tammela, *Opt. Express* **14**, 11539 (2006).
8. T. Arai, K. Ichii, S. Tanigawa, and M. Fujimaki, *Proc. SPIE* **7914**, 79140K (2011).
9. S. Jetschke, A. Schwuchow, S. Unger, M. Leich, M. Jäer, and J. Kirchhof, *Opt. Mater. Express* **3**, 452 (2013).
10. P. Jelger, M. Engholm, L. Norin, and F. Laurell, *J. Opt. Soc. Am. B* **27**, 338 (2010).
11. H. Hosono, M. Mizuguchi, L. Skuja, and T. Ogawa, *Opt. Lett.* **24**, 1549 (1999).
12. S. Agnello, M. Cannas, F. Messina, L. Nuccio, and B. Boizot, *J. Non-Cryst. Solids* **355**, 1042 (2009).
13. M. Leich, S. Jetschke, S. Unger, and J. Kirchhof, *J. Opt. Soc. Am. B* **28**, 65 (2011).
14. H. Gebavi, S. Taccheo, D. Tregoat, A. Monteville, and T. Robin, *Opt. Mater. Express* **2**, 1286 (2012).
15. X. Fu, L. Song, and J. Li, *Nucl. Instrum. Meth. B* **330**, 7 (2014).
16. S. Liu, M. Wang, Q. Zhou, S. Feng, C. Yu, L. Wang, L. Hu, and D. Chen, *Laser Phys.* **24**, 65801 (2014).
17. S. Liu, S. Zheng, C. Tang, X. Li, W. Xu, Q. Sheng, and D. Chen, *Mater. Lett.* **144**, 43 (2015).
18. Y. Shen, Q. Sheng, S. Liu, W. Li, and D. Chen, *Chin. Opt. Lett.* **11**, 051601 (2013).
19. K. M. Davis, A. Agarwal, M. Tomozawa, and K. Hirao, *J. Non-Cryst. Solids* **203**, 27 (1996).
20. S. Liu, H. Li, Y. Tang, and L. Hu, *Chin. Opt. Lett.* **10**, 081601 (2012).
21. A. Baraldi, E. Buffagni, R. Capelletti, M. Mazzer, S. Brovelli, N. Chiodini, A. Lauria, F. Moretti, A. Paleari, and A. Vedda, *J. Non-Cryst. Solids* **353**, 564 (2007).
22. J. E. Shelby, *J. Appl. Phys.* **50**, 3702 (1979).
23. D. L. Griscom, *J. Non-Cryst. Solids* **68**, 301 (1984).
24. E. M. Birtch and J. E. Shelby, *J. Non-Cryst. Solids* **349**, 156 (2004).
25. L. Skuja, *J. Non-Cryst. Solids* **239**, 16 (1998).
26. S. Agnello, G. Buscarino, F. M. Gelardi, and R. Boscaino, *Phys. Rev. B* **77**, 195206 (2008).
27. D. L. Griscom, *J. Non-Cryst. Solids* **64**, 229 (1984).
28. J. E. Shelby, *J. Non-Cryst. Solids* **179**, 138 (1994).
29. L. Nuccio, S. Agnello, and R. Boscaino, *Appl. Phys. Lett.* **93**, 151906 (2008).
30. Y. Kawaguchi and N. Kuzuu, *J. Appl. Phys.* **80**, 5633 (1996).